06

Postgrowth regime optimization of temperature and pressure reduction in HPHT-diamond crystal growth method

© N.I. Alekseev,[1,3] A.P. Broyko,[1] I.V. Klepikov,[2] A.V. Koliaidin,[2] I.V. Oreshko,[1,3] A.V. Solomnikova[1]

[1] St. Petersburg State Electrotechnical University LETI,
197022 St. Petersburg, Russia
[2] Almaz Scientific and Production Complex,
197706 Sestroretsk, Saint Petersburg, Russia
[3] Ioffe Institute,
194021 St. Petersburg, Russia
e-mail: NIAlekseyev@yandex.ru

Received September 27, 2024
Revised September 27, 2024
Accepted September 27, 2024

Along with exceptional strength characteristics, typical of the diamond is significant brittleness. In particular, an appreciable fraction of diamonds grown using HPHT technology, crack when the rigid P-T conditions inherent to the crystal growth process are gradually reduced. The cause of cracking is excessive stresses associated with the deficiency of plastic properties of the diamond growth medium at certain stages of P-T reduction. A significant contribution to the crystal cracking probability can also be made by the insulating container which encorporates the growth medium and a part of the heating circuit. The paper considers the possibilities of minimizing the mechanical stress in the growth cell and, consequently, in the diamond by choosing the optimal trajectory of the pressure and temperature reduction.

Keywords: high volume cubic press, diamond cracking, ductility of cast iron, ductility of solid catalyst.

DOI: 10.61011/TP.2025.02.60815.278-24

Introduction

Diamond electronics is currently a quickly advancing power and microwave electronics sector [1–3]. This study is concerned with a sufficiently substantial problem of HPHT (high pressure high temperature) diamond synthesis technique that is generally well established — diamond preservation with relaxation of quite rigid synthesis conditions (pressure of 5−6 GPa, temperature of 1750−1850 K). Orientation of cracks that are formed in such conditions is varying, but doesn't correspond to the (111) cleavage plane in a diamond. In post-growth loading conditions, primarily vertical and horizontal cracks are formed (with respect to diamond positions in a growth cell). Figure 1 shows type IIa HPHT-diamond with vertical cracks crosscutting the crystal from seed to tip. Orientations of such cracks are nearest to the (110) plane, but their shape is curved and the fracture that is formed on the crack surface is undulating and irregular. In the case of „horizontal" cracks, their orientation is close to the (100) plane, but the morphology and shape are identical to „horizontal" ones. As is commonly known, a diamond has no any cleavage in these orientations, and the fracture probably results from sharp and directional pressure.

The problem of cracking is important for the current HPHT process variables and, particularly, in transition to higher pressures. This transition makes it possible to grow larger crystals in a wider temperature range as can be seen from the HPHT synthesis diagram (Figure 2, the diagram is the average with respect to experimental data in [4–6]).

Better understanding of the cracking mechanism will make it possible to highlight those process factors that facilitate the mechanism. Such factors may include a growth cell container material, reinforcement and particular reduction dynamics of the pressure p and temperature T with time. The latter factor is corrected, if required, most easily, while the configuration and selection of other materials in the established technique are particularly hindered.

In particular, pyrophyllite (PP) is a well known pressure transfer medium that simultaneously ensures effective heat insulation. This material is unique in that it changes into viscous liquid when ultrahigh pressure is applied [7,8], however, according to the practical experience, it loses its plastic properties during long-hour holding of a diamond growth cell in the HPHT conditions. Potential PP replacement with other materials that are basically known goes beyond

Figure 1. Crystals with horizontal (a) and vertical (b) cracks.

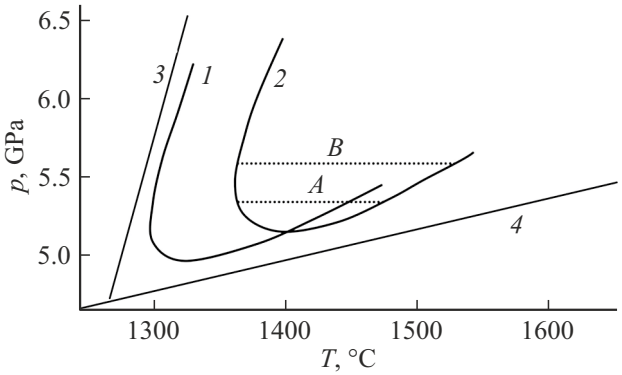

Figure 2. Schematic diagram $p-T$ of diamond crystallization region growth in the HPHT technique. *1, 2* — diamond growth region boundaries with various catalyst compositions of melt; *3* — catalyst melting boundary in the catalyst–carbon eutectic; *4* — boundary between the diamond (above the boundary) and graphite (below the boundary) stability regions. Increase in the operating pressure from level „*A*“ to level „*B*“ increases the allowable temperature range of diamond growth conditions and the process stability.

currently existing technical proposals, however, contribution of plastic properties of a medium, that is external with respect to the catalyst volume, to destruction or preservation of diamonds shall be also able to be evaluated.

Examination is complicated by the fact that plastic and other properties of a catalytic medium, that provides diamond growth to diamond seeds, are not known in any reliable way. Moreover, it is not possible to detect diamond integrity until normal conditions are achieved.

Features of the process that specify discussions in this work are applicable to a commercial large-size single-crystal diamond production technique (up to 150 karats, if the growth cell contains a single diamond seed and a single diamond is to be grown).

At early experiment stages, the problem was solved by generally uniform reduction of pressures and temperatures when there are additional „process shelves“ on which p, T were constant and then decreased stepwise. However, according to our examination, this solution is far from optimum.

This work is focused on the attempt to find conditions providing the lowest mechanical load both on the catalytic medium and on the PP container in a complex transient process when rigid parameters that exist by the time of diamond growth completion are reduced (hereinafter referred to as reduction for brevity).

1. Some features of the HPHT technique and possible causes of diamond cracking

Particular conditions and parameters of the simulated diamond production technique are as follows. For the HPHT process, the side of the cubic growth cell in cubic high-pressure presses (China) was approx. 50 mm, operating diamond synthesis pressure and temperature are (5.5–6) GPa and (1750–1850) K, respectively. These conditions are quite standard in the production process developed at Research and Production Company „Almaz“ in Sestroretsk.

A PP container layout with a diamond growth cell is shown in Figure 3. During the synthesis process, the container is subjected to the hard-alloy piston pressure (not shown in Figure 3) with pressure plate dimensions (50–60) mm. Besides the growth cell, the container also contain dolomite inserts for heat insulation, a heating circuit consisting of thermally expanded graphite, and a double MgO and steel enclosure with internal growth volume.

Layout of the cubic growth cell and reinforcement that partially envelopes the cell is shown in Figure 3 and is quite typical. Other configurations and layouts of the insulating layers around the cell [9–13] differ only in the layer sizes and material, which is nonessential for our discussion.

Difference in the thermal expansion coefficient (TEC) of diamond α_{diam} and solid metallic catalyst α_{cat} is an obvious and, in some sense, trivial cause of cracking. This difference can be easily considered in the simplest model of a spherical hard core of a diamond placed inside the spherical envelope of the catalyst material. In the absence of the core, the internal radius of the cooled spherical catalyst, that has no initial mechanical stresses and is not subjected to external pressure, decreases from r_{int} (equal to the initial diamond radius) to a smaller value of $r'_{\text{int}}(1-\alpha_{\text{cat}}\mathscr{P})$, where $\mathscr{P}$ is the temperature variation.

When there is a hard diamond core with low TEC, this radius is even smaller $\bar{r}'_{\text{int}} < r'_{\text{int}}$. The stress component σ_{rr} in the catalyst along the outline of contact with the diamond is approx. $\bar{\text{E}}_{\text{cat}}\left(\bar{r}'_{\text{int}} - r_{\text{int}}(1-\alpha_{\text{cat}}\mathscr{P})\right)$; $\bar{\text{E}}_{\text{cat}}$ is

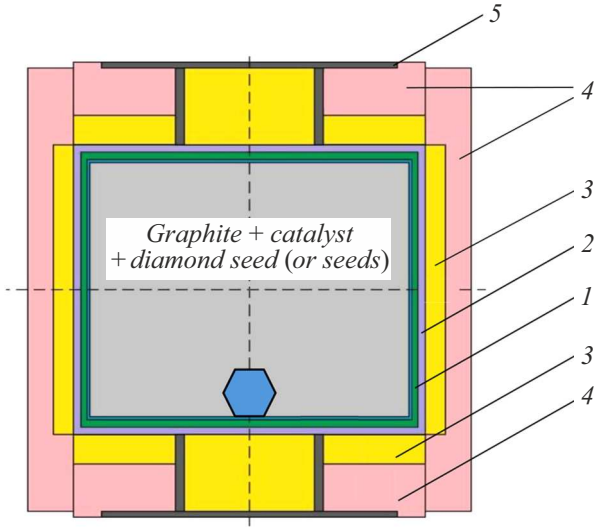

Figure 3. PP container layout: *1* — MgO layer, *2* — graphite, *3* — heat insulating dolomite layer, *4* — PP, *5* — steel electrodes. Internals of the diamond growth cell is shown gray and without details.

effective Young's modulus of the catalyst taking into account the tangential tension of the catalytic sphere and including Poison's ratio. In mechanical equilibrium condition, equality of σ_{rr} to that of the diamond gives

$$\bar{\mathrm{E}}_{\mathrm{cat}}\left(\bar{r'}_{\mathrm{int}} - r_{\mathrm{int}}(1-\alpha_{\mathrm{cat}}\mathscr{P})\right) = \bar{\mathrm{E}}_{\mathrm{diam}}\left(r_{\mathrm{int}} - (1-\alpha_{\mathrm{diam}}\mathscr{P}) - r'_{\mathrm{int}}\right).$$

Deriving r'_{int} from this, we get

$$(\sigma_{rr})_{r=\bar{r'}_{\mathrm{int}}} = \bar{\mathrm{E}}_{\mathrm{diam}}(r'_{\mathrm{int}} - \bar{r}_{\mathrm{int}}) = \frac{\bar{\mathrm{E}}_{\mathrm{cat}}\bar{\mathrm{E}}_{\mathrm{diam}}(\alpha_{\mathrm{cat}} - \alpha_{\mathrm{diam}})}{\mathrm{E}_{\mathrm{cat}} + \mathrm{E}_{\mathrm{diam}}}\mathscr{P} \approx \bar{\mathrm{E}}_{\mathrm{cat}}(\alpha_{\mathrm{cat}} - \alpha_{\mathrm{diam}})\mathscr{P}$$

(the last approximate equation takes into account that $\mathrm{E}_{\mathrm{diam}} = 1100\,\mathrm{GPa} \gg \mathrm{E}_{\mathrm{cat}} = (200-300)\,\mathrm{GPa}$). Since the TEC- difference between the diamond and catalyst is in the order of TEC values themselves, i.e. 10^{-6}, when the temperature decreases even by 10^3 K, the radial stress shall not exceed few MPa. The same is true for tangential stress. Therefore, the *TEC*-difference between the diamond and catalyst hardly causes cracking and other causes shall be analyzed. They include numerous possible defects inherited from seeds in the HPHT technique [1]. Another cause may include growth inclusions of atoms, catalyst material clusters or oxides [14,15]. However, this seed preparation technique has been adequately established. Moreover, it is hardly possible to influence the structure of defects in the diamond itself both when p and T increase and decrease, and these defects may be very various. Therefore, we assume that by the time of growth completion the diamond is free of defects (as well as of cracks). Then, the discussion naturally focuses on the fast-setting catalyst medium where the diamond resides during the whole reduction time.

2. Theoretical model

2.1. Key terms of plasticity theory used in the model

According to the loss of weight of graphite which is the source of carbon for diamond growth, it can be easily evaluated that, by the time when the temperatures and pressures start decreasing, the carbon percentage in the catalyst reaches at least $(5-10)$ mass%. Therefore the catalyst medium will be correlated with cat iron especially as, at the p and T reduction stage, it copmpletely loses its catalytic role.

The point of reduction, i.e. diamond growth conditions ($p \sim 5.5$ GPa, $T \approx 1750-1800$ K), is close to the liquidlines for iron and transition metals in the iron group (Ni–Co according to book [16]). Therefore, the initial reduction path point on p, T phase diagram is assigned to the solid phase of the catalyst and compared with the diagram of a pure substance — iron, especially as the catalyst composition is nonuniform and may be assessed only approximately. Then, when p and T decrease from the initial growth values (bullet S in the top right corner of Figure 4) to normal conditions (origin of coordinates), initial section of the reduction path goes through a region corresponding to highly plastic state. For evaluation, an easy case of S.N. Zhurkov's theory may be used to determine the effective plastic deformation time τ_{relax} (or plastic fracture or cracking) as follows [17]:

$$\tau_{\mathrm{relax}} = \tau_0 \exp\left((U_0 - \gamma\sigma(p,T))/T\right), \qquad (1)$$

where σ is the generalized system stress, $(U_0,\ \gamma)$ correspond to the above-mentioned processes; γ is the activation volume. For plastic deformation, the energy U_0 is close to 2/3 of the evaporation energy, the „seed“ time τ_0 has an order of inverse atomic vibration frequency in lattice, i.e. 10^{-13} s.

At a stress limit that is denoted as Zhurkov's stress $\sigma_{\mathrm{Zh}} = U_0/\gamma$, the activation barrier $U_0 - \gamma\sigma(p,T)$ vanishes. When σ_{Zh} is correlated with the plastic limit $\sigma_T(p,T)$ catalyst material (that is considered to be known), we get line *1* on the p, T plane (Figure 4). To the right of this line, the plastic state is established immediately, and the material may be considered as extremely plastic.

For some metals, σ_{Zh} may be reliably determined. Thus, in [18], $U_0 = 3.8$, 4.4, 3.6, 5.7 eV are proposed or Ni, Fe, Cu, Pt, respectively. Values of γ for Ni, Cu, Pt are equal to 0.7, 1.6, 5.2 nm^3. Then, σ_{Zh} for Ni, Cu, Pt are equal to 851.8, 354 and 1726 MPa. According to indirect data of the same paper [18], for iron $\sigma_{\mathrm{Zh}} = (865-880)$ MPa.

Initial data on $\sigma_T(p,T)$ is extremely poor, though at normal pressure and temperatures up to 1000 K, $\sigma_T(p,T)$ for cast irons and steels are a quite standard characteristic: curves $\sigma_T(p,T)$ droop steadily. With focus on the

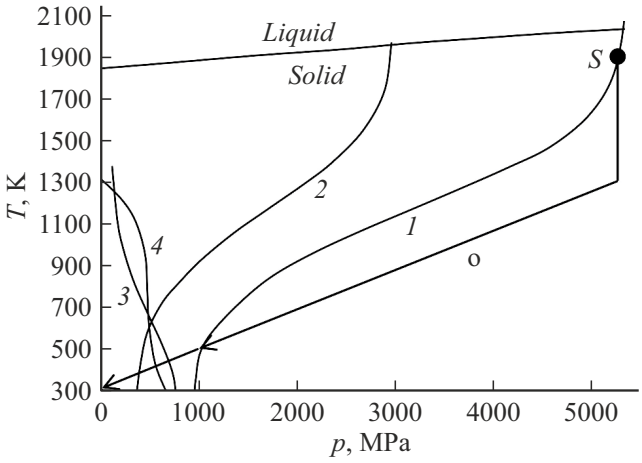

Figure 4. Typical curves of fundamental change in the catalyst properties in the p, T diagram and the optimum path of reduction from high values of p, T inherent in the diamond synthesis to normal values — line „o“ (optimal). *1* — line $\sigma_T(p,T) = \sigma_{\mathrm{Zh}}$; *2* — line $\sigma_T(p,T) = 0.6\sigma_{\mathrm{Zh}}$; *3* — $\sigma_T(p,T) = p$; *4* — $\tau_{\mathrm{relax}} = 1$ s; top straight line — phase interface; bullet S — stationary values of p, T during diamond growth.

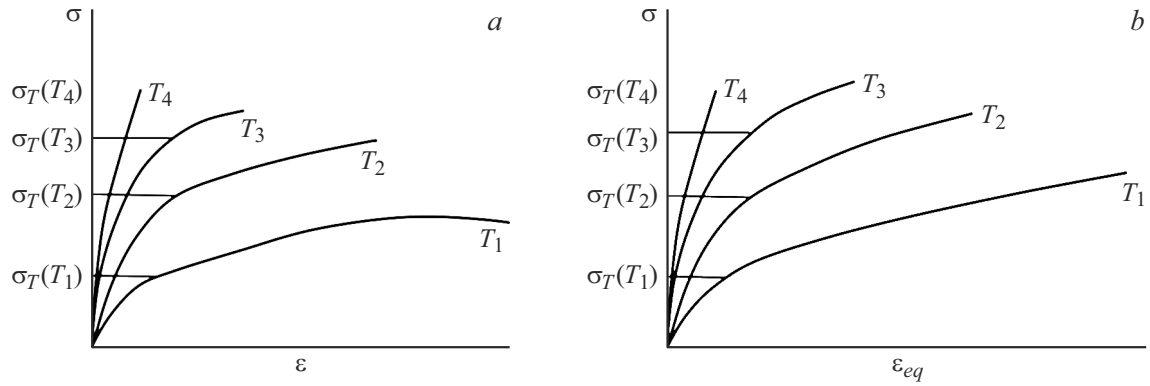

Figure 5. Qualitative behavior of plastic properties of a cast-iron-like material in linear tension (a) and in uniform compression (b) depending on the temperature [19]: $T_1 > T_2 > T_3 > T_4$; equivalent compression ε_{eq} is set equal to $\varepsilon/3$.

achievement of qualitative conclusions and assuming that at temperatures up to 2000 K $\sigma_T(p, T)$ tends to some constant value of $\sigma_T(p = p_n = 1\,\text{atm}, T_\infty)$, we assume the Gaussian shape of decay curve

$$\sigma_T(p_n, T) = \sigma_T(p_n, T_\infty) + \big(\sigma_T(p_n, T) - \sigma_T(p_n, T_\infty)\big)E,$$

$$E = \exp\big(-(T - T_n)/(T_1 - T_n)^2\big), \qquad (2)$$

where T_∞ is the conventional upper temperature limit, „n“ hereinafter corresponds to normal conditions.

Expression (2) implies that the plastic limit decreases with the temperature growth by a factor of approx. e; the adjustable temperature T_1 is set to 980 K. As shown in the typical s–s diagram (strain–stress, Figure 5, a), such equation doesn't contain all required information because the decrease in σ_T with the temperature growth is followed by the growth of „placticity plateau“ in the deformation ε. Therefore, the temperature effect on plasticity is ambiguous.

Unfortunately, the known s–s diagrams for cast irons are limited only by bar tension–compression experiments. Using the diagrams, it is quite difficult to predict plastic medium behavior during uniform compression of the growth cell and at the same time when hard inclusions in the form of diamond (or a group of diamonds) act on the medium from inside. This study assumed that horizontal sections of $\sigma(\varepsilon)$ are converted into inclined sections (Figure 5, b) and their end positions (plastic fracture) move towards higher equivalent values of $\varepsilon_{eq} \sim \varepsilon/3$. It was further assumed that at temperatures much higher than room temperature T_n, σ_T in compression qualitatively characterizes this quantity in uniform compression as well.

Data on the dependences of $\sigma_T(p, T)$ (or proportional quantities such as fractioning activity or threshold σ_{frac}) on pressure at room temperature T_n for some cast irons and steels collected in [19] show that curves $\sigma_T(p)$ are straight (or almost straight) up to a pressure of about 1 GPa:

$$\sigma_T(p, T_n) = \sigma_T(p_n, T_n) + \alpha_n(p - p_n). \qquad (3)$$

For calculation, $\sigma_T(p_n, T_n)$, α_n at $T_n = 300$ K are set to: $\sigma_T(p_n, T_n) = 300$ MPa; $\alpha_n = 0.6$ at T_∞ $\alpha_\infty = 0.6$, pressures as in $\sigma_T(p, T_n)$ are given in MPa.

A limit of 1 GPa in (3) is obviously insufcient. Studies of metal, glass and mineral properties conducted by P.W. Bridgman in the 30s–40s [19], that covered external pressures up to 30,000 atm, pointed out the following: despite the growth of material plasticity, uniform pressure cannot exceed the strength and plasticity in an unlimited way. On the other hand, not only steels, but also black cast iron, phosphorous bronzes, beryllium and marble, are reinforced at pressure higher than 2.5 GPa. For pressure extrusion of bars, pressures higher than 1 GPa are also used, and there is no information whether brittleness increases.

Plastic characteristics at ultrahigh pressures could have been decreasing at the approach to the critical point on the melt–metal phase transition, i.e. at the temperature above which the melt cannot be hardened at any pressure. However, the estimated critical pressure for transition metals in the iron group is not lower than 1 million atm [20]. This is higher than the traditional diamond anvil conditions, apart from the HPHT conditions. On the basis of the foregoing, the plasticity limit was set as (3) at all T, including also $T = T_\infty$:

$$\sigma_T(p,\ T_\infty) = \sigma_T(p_n,\ T_\infty) + \alpha_\infty(p - p_n). \qquad (4)$$

Correlation between the temperature-pressure curve slope at T_n and conventional extremely high temperature T_∞ was set as

$$\sigma_T(p_n,\ T_\infty) = \sigma_T(p_n,\ T_n)/e. \qquad (5)$$

As a whole, $\sigma_T(p,\ T)$ was set by combining (3)–(5):

$$\sigma_T = \sigma_{n,\infty} + \alpha_\infty(p - p_n) + \big(\sigma_{n,n} - \sigma_{n,\infty} + (\alpha_n - \alpha_\infty)(p - p_n)\big)E, \qquad (6)$$

where E is introduced into (2).

2.2. Typical lines of fundamental change in catalytic metal properties on the (p, T)-plane

We now turn to qualitative discussion of $\sigma_T(p, T) = \sigma_{\text{Zh}}$ on line *1* (Figure 4). Intersection of this line with

the liquid–solid body phase interface at pressure close to 5.5 GPa (i.e. operating pressure of diamond growth in a particular system) is quite random; the p, T reduction path not necessarily starts on line *1*.

As mentioned above, the material is as plastic as possible to the right of line *1*. To the left of line *1*, there is a region that may be called as an activated plasticity region, i.e. finite time is required to determine plasticity. If plastic properties on some reduction path inside this region weaken, then instant exceedance of stress over plasticity limit in an earlier point of time may be higher than the strength capabilities of the catalyst. Excessive stress is transferred to the diamond, thus, increasing the probability of its fracture.

There is an elastic region to the left of the activated plasticity region. Due to lack of information, its right boundary can be set in different ways. Constancy of σ_{lin}/σ_T (for example, $\sigma_{lin}/\sigma_T = 0.6$) is suggested, where σ_{lin} is the limit of linearity of the s–s curve. For a large number of cast irons, this corresponds to reality and makes it possible to plot a line identical to line *1* (Figure 4) where σ_{Zh} is replaced with $0.6 \cdot \sigma_{\text{Zh}}$ (line *2*):

$$0.6 \cdot \sigma_{\text{Zh}} = \sigma_T(p, T). \tag{7}$$

The second method is based on the fact that the stress is proportional to pressure on the linear section of s–s and isn't much different from pressure at the linear section end (curve *3*):

$$p = \sigma_T(p, T). \tag{8}$$

Besides curves *2* and *3*, the highly activated plasticity region was evaluated in one more way. p, T at which the plasticity delay time τ_{relax} in equation (1) was equal to the set value, e.g. 1 s (Figure 4, curve *4*) were determined.

Curves *2–4* together with curve *1* form a kind of „canyon“ in the region of low p, T, which must be intersected by the p, T reduction path. As the plastic properties of the catalyst decrease sharply at the approach to the left edge of the „canyon“ this is the region hat shall be considered as extremal.

Until the left edge of the „canyon“ is reached, the optimum reduction path shall leave line *1* above of itself. At any time, the catalyst immediately comes to the plastic state and there is the least probability of diamond fracture. However, the condition of non-inclusion into the activated plasticity region for the optimum p, T reduction path may contradict with other desired diamond preservation conditions. Therefore, it is necessary to determine quantitatively which paths inside such region expose the diamond to higher danger.

Initially to evaluate such danger, the ratio of instant pressure to plasticity limit in an earlier point of time $t - \tau_{\text{relax}}$; ($\theta(t)$ is the Heaviside θ-function)

$$D = (p/\sigma_T)\Theta(p/\sigma_T - 1), \quad \sigma_T = \sigma_T(p, T)_{(t-\tau_{\text{relax}})} \tag{9}$$

was used as a parameter characterizing the diamond fracture probability.

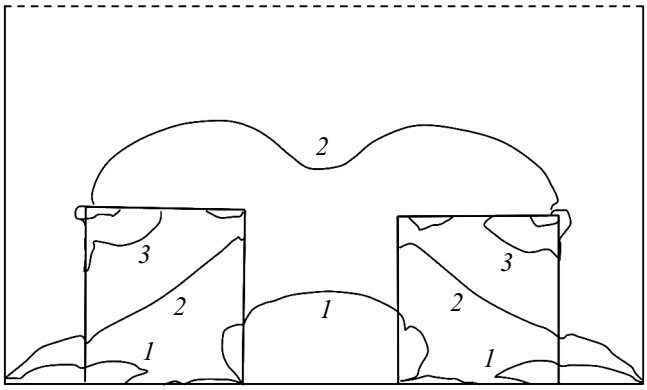

Figure 6. Stress field σ_{xx} in the 40×40 mm growth cell. There are two 7×7 mm diamonds on the bottom of the cell. Catalytic medium in the cell with the applied pressure of 1 GPa is set close to an ideally plastic medium [21]. In the region between diamonds that is partially shielded from external pressure, the stress is reduced, increased inside diamonds on the sides facing the container sides and distributed over the diamond quite unevenly. The figure reproduces quite a faint picture obtained in ANSYS 13.0. The scale bar under the figure is 20 mm. Stress isobars correspond to (MPa): *1* — 425, *2* — 700, *3* — 1800.

Introduction of D partially compensates the lack of information about the plastic properties of the catalyst in complex deformation and makes it possible to avoid mapping of numeric deformation and stress field for each point on the path (p, T) (especially as such field always describes the already established plasticity). Calculation of the stress field in ANSYS.13 is illustrated in Figure 6.

Variation of $D(t)$ for several reduction paths from the initial point S on curve *1* (Figure 4) until the elastic catalyst region is achieved was calculated at the same reduction time 20 min. Reduction paths on the p, T plane are shown in Figure 7, variation of D is shown in Figure 8. On curves *1′–3′* in Figure 9, the pressure decreased uniformly with time from the start $p_s = 5250$ MPa to final $p_f = 514$ MPa corresponding to the elastic region boundary.

The start temperature T_s was 1888.2 K, and the final temperature varied: $T_f = 516.5$ on curve *1′*, 700 on *2′*, 1000 K on *3′*. The temperature on these three curves (*1–3*), as well as the pressure, decreased uniformly with time. On curve *5′*, the temperature decreased to $T_f = 516.5$ K first at a growing rate with respect to p, and then at a slow rate; on curve *4′* — vice versa. Numbers of curves in Figure 7, 8 are the same as on curves in Figure 5.

In Figure 9, relaxation time variation is plotted for curves *1–3*. It can be seen that the plastic state development decay is small to nearly the elastic region boundary and becomes significant only at the path end, when the external pressure decreases by a factor of (5–6). Variation of static plastic properties becomes more significant. A gently sloping temperature decrease path is most dangerous (curves *3′, 4′*), in Figure 7, 8), when the plastic property growth due to temperature reduction fails to compensate weakening of

the same properties in due time due to reduction of p (Figure 5).

D is maximum in the beginning of the path (i.e. in early points of time) and this is the section where the pressure shall be first reduced slowly and the temperature shall be reduced much faster. However, the region at the approach to the elasticity region boundary also may be dangerous. Mechanical stresses will be compared with the fracture limitσ_{fract}, rather than with the plasticity limit, which is probably more correct. If curves $1'-5'$ are replotted (Figure 8) as ratios D' of pressure to σ_{fract}, then they will numerically coincide with curves D only when the plasticity limit σ_T and fracture limit σ_{fract} are varied proportionally.

If the fracture limit decreases with temperature reduction faster than the plasticity limit (as in Figure 5, b), then the shape of curves is much flatter compared with curves $D'(t)$ (Figure 10, curve $3'''$), and the catalyst fracture risk still exists throughout the cooling and pressure relief path.

The literature data on σ_{fract} and σ_T are extremely scattered. Therefore, according to little known data and assuming the start pressurep_s and final pressure p_f as fixed values, we supposed that between the start and final temperaturesT_s and T_f $\sigma_{\text{fract}}/\sigma_T$ varies linearly as the catalyst cools down as follows

$$\sigma_{\text{fract}}/\sigma_T = (\sigma_{\text{fract}}/\sigma_T)_s - \left[(\sigma_{\text{fract}}/\sigma_T)_s - (\sigma_{\text{fract}}/\sigma_T)_f\right] \times (T - T_s)/((T_f - T_s)$$

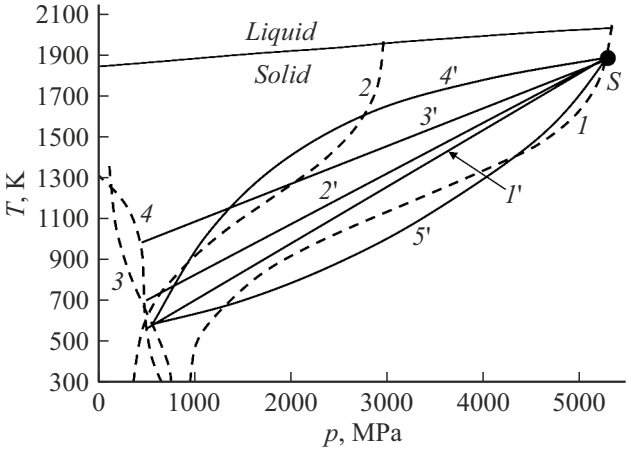

Figure 7. Pressure and temperature reduction paths to the elastic region boundary in the activated plasticity region (curve *1*). Along curves $1'-3'$, the temperature and pressure droop linearly with time during 20 min. On curves $4', 5'$, the pressure decreases linearly, the temperature decreases according to $T = T_s + (T_f - T_s)\left[(p - p_s)/(p_f - p_s)\right]^2$ and $T = T_f + (T_s - T_f)\left[(p - p_f)/(p_s - p_f)\right]^2$, respectively.

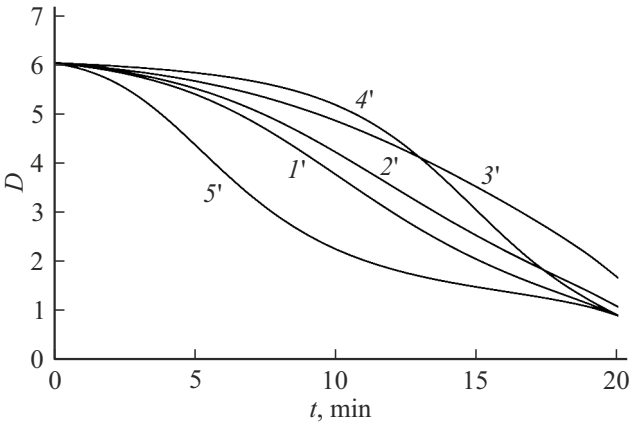

Figure 8. Variation of the fracture parameter D with time. Curves $1'-5'$ correspond to the p, T reduction curves in Figure 5 with the same numbers.

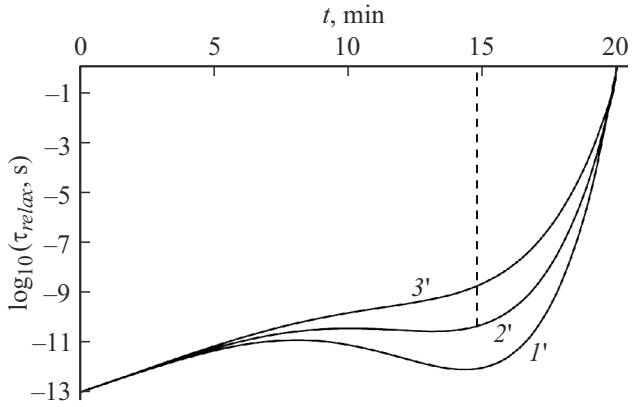

Figure 9. Relaxation time variation for curves $1'-3'$. They correspond to reduction curves p, T shown in Figure 6 with the same numbers. Dashed line — conventional start of strong effect of container cracks on the plastic state of the catalyst.

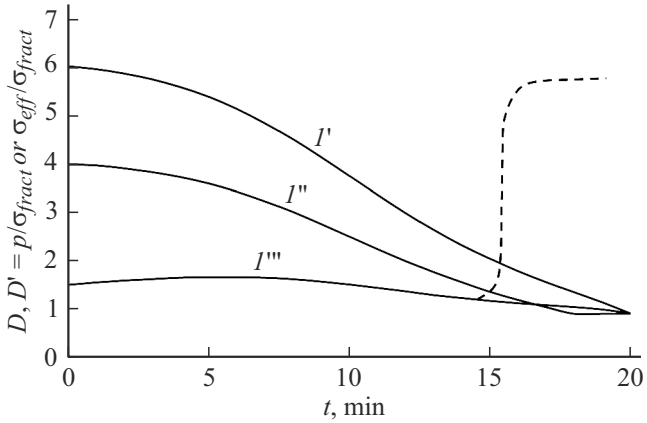

Figure 10. Variation of fracture parameters D and D' at the activated plasticity stage. Curve $1'$ corresponds to $1'$ in Figure 6, 7. On curves $1''$ and $1'''$ corresponding to the same process, D' is defined as $D' = p/\sigma_{\text{fract}}$; $\sigma_{\text{fract}}/\sigma_T = \text{const} = 1.5$ on curve $1''$, and varies linearly according to $\sigma_{\text{fract}}/\sigma_T = (\sigma_{\text{fract}}/\sigma_T)_s - \left[(\sigma_{\text{fract}}/\sigma_T)_f - (\sigma_{\text{fract}}/\sigma_T)_f\right] \times (T - T_s)/(T_f - T_s)$ on $1'''$ from the start value — $(\sigma_{\text{fract}}/\sigma_T)_s = 4$ to the final values $(\sigma_{\text{fract}}/\sigma_T)_f = 1$ as the catalyst cools down. Effective stress growth associated with the presence of cracks in the container in reduced plasticity conditions is shown dashed.

from the start value $(\sigma_{\text{fract}}/\sigma_T)_s = 4$ to the final value $(\sigma_{\text{fract}}/\sigma_T)_f = 1$.

It is intuitive that, for practice, both the pressure and temperature reduction rates shall be preferably reduced significantly in the range $p = (0{-}6{-}1)$ GPa, where the plasticity delay becomes high (in the order of minutes); e.g. to spend 1 h for passing the $(1 \rightarrow 0.6)$ GPa section. This result is also derived from other considerations discussed below in Section 3.

At a lower pressure, the catalyst behavior becomes elastic. As shown below, the stress level now may be affected only by nonstationary temperature gradients GradT associated with sharp reduction of mean temperature $\bar{T}$ in the growth cell, but they can be reduced easily. Let's evaluate GradT.

Graphite heater and pistons (not shown in Figure 3) are the heating circuit elements of the growth cell, the insulating MgO layer and growth cell are the heat problem elements. The graphite heater, as well as the current-carrying circuit through the pistons, may be excluded straightway from the heat problem consideration. Power supplied to PP container is then released almost completely in the growth cell and thin MgO enclosure that has a lower thermal conductivity than the cell. Therefore, the stationary temperature distribution delay in the cell τ_{delay} is defined by the heat capacity c_{cat}, density ρ_{cat} and thermal conductivity œ_{cat} of the cell's catalytic material alone. By order of magnitude

$$\tau_{\text{delay}} \approx r_{\text{cell}}^2 \rho_{\text{cat}} c_{\text{cat}} / 2\text{œ}_{\text{cat}}, \tag{10}$$

and the nonstationary temperature gradient between the cell center and heat release point (graphite heater) is

$$\delta T \sim \tau_{\text{delay}} (d\bar{T}/dt). \tag{11}$$

c_{cat}, ρ_{cat} and œ_{cat} of the metal catalyst (iron) in normal conditions are set to 0.50 W/(cm·K), 7.5 g/cm^3 and 0.9 J/(g·K); a half r_{cell} of the cell side $2r_{\text{cell}}$ is $r_{\text{cell}} = 3$ cm. Taking into account the variation of these parameters depending on p, and T, $\tau_{delay} \sim 1$ min and $\delta T \sim 50$ K with uniform temperature reduction from 2000 to 500 K during 40 min. This is approximately corresponds to the stationary process temperature difference in the cell during diamond growth. At a lower reduction rate of T equal to 10 K/min (1000 K per 1.5 h), the nonstationary temperature effects are inessential and are not able to cause any significant stresses in the diamond.

Calculation of the stress field σ_{xx} in the diamond and catalyst for stresses that occur due to the difference in Young's moduli and TEC- of the diamond and catalyst in terms of the elastic problem (ELCUT 5.2) showed that the emerging stress is a little higher than the external pressure (by approx. 30% at the external pressure of 1 GPa and vertical temperature difference of 50 K), though it is actually concentrated mainly on the diamond.

2.3. Effect of plastic properties of the container and container-related restrictions on the p, T reduction path

Thus, neither „delayed plasticity“ nor temperature gradients even on the „hazardous“ section below 1 GPa lead to excessive tresses in the diamond and shall cause diamond fracture. However, the foregoing discussion didn't cover strength properties of the PP container with the growth cell. Container integrity makes almost no difference for the diamond integrity until the catalyst material is plastic. As shown in Figure 4, this is true up to ~ 1 GPa. But at a lower pressure, i.e. in elastic behavior region of the catalyst, it fully transfers overstresses induced in the external cell to the diamond. This is important if the PP container is not plastic and acquired cracks „in advance“ at pressure higher than 1.0 GPa.

The typical pattern of the breaking stress field σ_{xx} induced by a triangular crack 5 mm in depth and 3 mm in width on top in an elastic material is shown in Figure 11. It can be seen that the breaking stress on the crack bottom extends deep into the catalyst at least to the crack depth, and the effective stress width exceeds the transverse width of the crack approximately by an order of magnitude.

Figure 12 shows a stress field σ_{xx} initiated by thee cracks in the PP container — top, left and bottom (i.e. directly beneath the diamond) at comprehensive load of 1 GPa. Young's modulus and Poison's ratio of the container are set to 300 GPa and 0.25. Dimensions of the diamond are 7×7, height of the growth cell is 20 mm, width of the growth cell is 3 mm. It can be seen that the maximum breaking stress induced in the diamond is concentrated at the bottom, i.e. above the crack.

Given there is a problem to ensure the lowest probability of container cracking at the temperature and pressure reduction stage provided that such cracks haven't occurred yet during the diamond growth times. As there is hardly any information on the strength properties of PP that was fully dehydrated and lost its plastic properties, we assume that the volume and content of the hard PP enclosure wasn't changed. Then reduction of the catalyst volume inside the PP leads to reduction of the pressure applied to the catalyst from inside. Consequently, in the parameter behavior

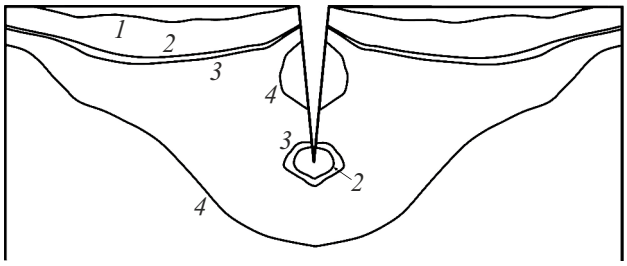

Figure 11. Stress component σ_{xx} in the elastic catalyst material with Young's modulus of 200 GPa simulated by hard iron at a load of 1 GPa on the top of the material (ELCUT 5.2). Points on the isobars of σ_{xx} correspond to (10^8 Pa): *1* — 3.6; *2* — 2.15; *3* — 1.9; *4* — 0.4.

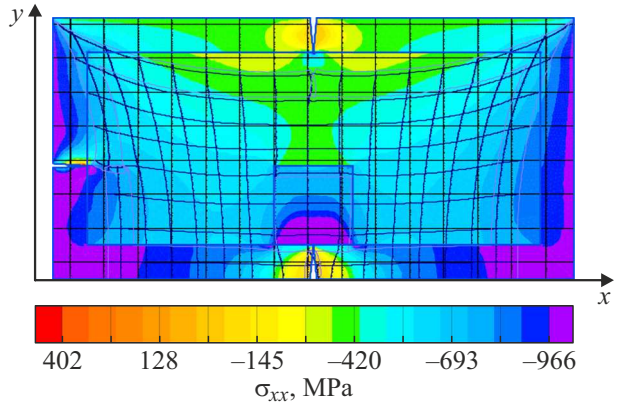

Figure 12. Stress field σ_{xx} initiated by thee cracks in the container — on the top, at the left and at the bottom beneath the diamond at comprehensive load of 1 GPa (dark-blue, ELCUT 5.2).

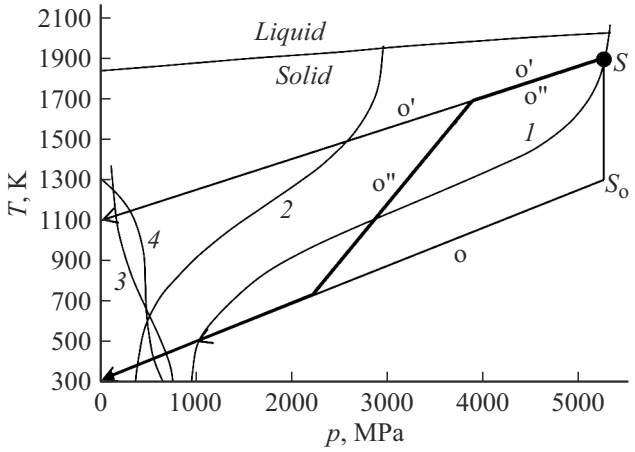

Figure 13. p, T reduction paths that ensure the minimum probability of overstresses in the catalyst (o) and PP container integrity (o'), respectively.

that is optimum for container preservation, the external pressure shall decrease in the same rate. While, according to thermodynamics, reduction of the internal pressure p_{int} associated with cooling is

$$dp_{\text{int}}/dT \approx (\partial p/\partial T)_v = -(\partial p/\partial V)_T(\partial V/\partial T)_p = 3\alpha_{\text{cat}}/\varsigma, \quad (12)$$

where ς is the isothermal catalyst compressibility. For hard iron in normal conditions, $dp_{\text{int}}/dT \approx (\partial p/\partial T)_v = -(\partial p/\partial V)_T(\partial V/\partial T)_p = 3\alpha_{\text{cat}}/\varsigma$, $\varsigma = 0.6 \cdot 10^{-6}$ 1/atm, and the internal pressure reduction rate is $dp_{\text{int}}/dT \sim 50$ atm/K, i.e. the pressure reduction is approx. 10^5 atm with general cooling of ~ 2000 K for all the time. This is only twice as much as the ratio of mean pressure and temperature reduction rates.

Therefore the reduction path that is optimum for PP integrity is almost entirely within the activated plasticity region (path o' in Figure 13) and has very small slope. On the contrary, to achieve the reduction path that is optimum for catalyst integrity, the initial cooling section shall be passed without pressure reduction (section $S \to S_o$); however, the container fracture risk is maximum.

3. Experiment and its comparison with modeling results

Thus the catalyst and PP container integrity requirements agree very poorly. When the container is not broken and the breaking impacts on the diamond are associated with the plastic catalyst medium, then the fracture probability reduction problem is solved easily,as it follows from the foregoing. When the contained is broken, then some diamonds are in an additional stress field that exceeds the pressure by some factor of$M > 1$. This stress exceeds the plasticity limit at current (p, T), that, beginning from some time, is established very slowly (dashed line in Figure 9). Therefore, during all the time after sharp growth necessary for τ_{relax} and until transition to the linear mode (at the pressure about $p_{\text{lin}}/(1+M)\,D'$ is much higher than in other points of time (dashed line in Figure 10).

Composite probability of diamond fracture due to the lack of catalyst's plastic properties and container fracture will be described by the integral fracture parameter $\langle D' \rangle$. Let's write it in terms of Zhurkov's theory in the form that generalized equation (1), i.e

$$\langle D' \rangle \sim \left(1 - \int_0^{t_1} \omega_{\text{cont}}^{\text{destr}}(t')dt'\right) \times \int_0^{t_1} \exp\left(\frac{\gamma\left(p - \sigma_{\text{fract}}(p(t), T(t))\right)}{T(t)}\right)dt + \int_0^{t_1} \omega_{\text{cont}}^{\text{destr}}(t')dt' \int_{t'}^{t_1} \exp\left(\frac{\gamma\left(Mp - \sigma_{\text{fract}}(p(t), T(t))\right)}{T(t)}\right)dt \quad (13)$$

as the sum of catalyst cracking probabilities with integral container during all the time and increased probability of such cracking starting from the container fracture time. In equation (13), t_1 is the time of p, T reduction from the start point S (Figure 4, 13) to the elasticity region boundary. As the second term becomes significant only in the vicinity of the „canyon“ (Figure 4), the effective stress included in the exponent is set equal to Mp. M shall be fitted. The second fitted parameter $p_{\text{cont}}^{\text{destr}}$ — „container fracture pressure“ – was associated with the container fracture probability $\omega_{\text{cont}}^{\text{destr}}$:

$$\omega_{\text{cont}}^{\text{destr}} = (\delta p/p_{\text{cont}}^{\text{destr}})\left(1 - \theta(\delta p/p_{\text{cont}}^{\text{destr}})\right) + \theta(\delta p/p_{\text{cont}}^{\text{destr}}), \quad (14)$$

expressed through the excess pressure δp. This probability was calculated by numerical integration of derivative dp_{int}/dT in (12) on the (p, T) reduction path.

According to (13) and (14), two target calculation functions were set — fraction of diamonds with cracks ω

corresponding to particular experiment (i.e. implanting diamond seeds and p, T reduction path), and fraction of integral containers. This made it possible to plot $p_{\text{cont}}^{\text{destr}}(M)$ and compare it with the actual fraction of broken containers (this fraction is very small and is about 20%). Then, comparing ω with $\langle D' \rangle$ that has obviously the same physical significance, M was found, at which curve $\omega(\langle D' \rangle)$ had the lowest dispersion and at the same time was as close as possible to the straight line. As almost any array of experimental points may be fitted to the straight line, the least-square sum at each trial value of M was minimized by fitting to a family of quadratic dependences crossing the „zero-axis“, and by selecting the most „straight“ one of them. Thus evaluated M was 1.8. It is significant that the experimental point arrays obtained with integral container fall on the same straight line as the points corresponding to the broken container. This means that only two explicit parameters — $p_{\text{cont}}^{\text{destr}}$ and M — were selected quite very successfully.

In any case, an „ideal“ o'' reduction path (Figure 13) shall pass between the straight line o' (lower container integrity boundary) and the activated plasticity region boundary (path *1* in the same figure). Movement velocity on this path shall be variable. Actually, the integral fracture parameter explicitly tends to infinity with infinite reduction deceleration (static fracture). At the same time, the plasticity establishment rate of the catalyst before entering the „canyon“ region in Figure 4, 13 (or to the left of the dashed line in Figure 9, 10) is high, and the container doesn't have plastic properties. Therefore, slowly conducted process above 1−1.5 GPa accomplishes nothing for keeping the „catalyst−container“ system integrity, and it preferable to perform this reduction quickly (less than 1 h) in the path range (For example, o''). On the contrary, the catalyst plasticity in the „canyon“ region in Figure 4, 13 (or to the right of the dashed line in Figure 9, 10) is established slowly, independently of the container state. Therefore, the range of $1.5 \rightarrow 0.6$ GPa shall be preferably passed at a minimum acceptable velocity from commercial considerations.

According to the foregoing, the velocity of passage through the elastic region of (p, T) lower than (0.8−0.6 GPa) is not critical. To minimize nonstationary temperature compression effects, is sufficient to set the reduction time on this section to 1 h.

Utilization of a container made from synthetic composite materials, rather than from pyrophyllite (though this technology is well established and familiar), gives even better result. In this case, the container integrity problem may be neglected, and path *1* in Figure 13 shall be considered as the optimum path.

Findings and conclusion

When pyrophyllite is used as a pressure transfer medium for the diamond growth cell, the optimum pressure and temperature reduction path is defined by the compromise between pyrophyllite container integrity and minimization of the stress level in the plastic medium of the catalyst. The first factor is substantial at high pressure and dictates comparatively faster pressure reduction than temperature reduction at least in the beginning of the reduction path on the (p, T) plane.

The second factor is more substantial in the transition region from the plastic state of the catalytic medium to the elastic state at a pressure of about 1 GPa; this transition region depends on temperature very weakly.

Compromise is achieved on type paths (shown in Figure 13) provided additionally that the transition pressure region is passed slowly.

When using the pressure transfer medium that has plastic properties, the optimum path implies faster temperature reduction than pressure reduction in the start high pressure region. The requirement of slow passage through the plastic property variation region of the catalyst medium (about 1 GPa) is still valid.

Funding

The study was performed under project № FSEE-2024-0005 (state assignment of the Ministry of Science and Higher Education of the Russian Federation No 075-00003-24-00).

Conflict of interest

The authors declare no conflict of interest.

References

[1] R.A. Khmel'nitskii, N.Kh. Talipov, G.V. Chucheva. *Sintetich-eskii almaz dlya elektroniki i optiki* (IKAR, M., 2017) (in Russian) S. Shikata. Diamond & Related Mater., **65**, 168 (2016).
[2] N.I. Alekseev, V.V. Luchinin. *Elektronika almaza* (Izd-vo SPbGETU „LETI“, SPb., 2020) (in Russian)
[3] S. Koizumi, H. Umezawa. J. Pernot, M. Suzuki (eds). *Power Electronics Device Applications of Diamond Semiconductors* (Woodhead Publishing Series in Electronic and Optical Materials, 2019)
[4] R. Li, M. Ding, T. Shi. J. Crystal Growth, **491**, 111 (2018). DOI: 10.1016/j.jcrysgro.2017.12.021
[5] X. Liu, X. Jia, X. Guo, Z. Zhang, H. Ma. Crystal Growth & Design, **10** (7), 2895 (2010). DOI: 10.1021/cg901168s
[6] X. Liu, X. Jia, C. Fang, H. Ma. Cryst. Eng. Comm., **18**, 8506 (2016). DOI: 10.1039/c6ce02034h
[7] L.A. Gordienko, Yu.A. Detchuev, V.I. Zadneprovsky, S.V. Kolodieva, O.P. Komarov, V.A. Laptev, D.G. Malova, N.I. Petrova, L.N. Romanov, M.I. Samoilovich, N.G. Sanzharlinsky, V.I. Khadzhi, L.I. Tsinober, L.M. Shterenlikht. *Sintez miner-alov* (Nedra, M., 1987), t. 1. (in Russian)
[8] Electronic source. Available at: https://ru.wikipedia.org/wiki/Pyrophyllite (description of physical properties)
[9] Q.G. Han, H.A. Ma, G.F. Huang. Rev. Sci. Instrum., **80**, 043505 (2009).

[10] Qi-Gang Han, Q.C. mBan, P.W. Zhu. J. Cryst. Growth, **422**, 29 (2015).
[11] Rui Li, B. Xu, Q. Zhang, X. Gu, G. Zheng, H. Ma, X. Jia. High Pressure Res., **36** (4), 575 (2016). DOI: 10.1080/08957959.1238915
[12] Y. Li, Y. Li, L. Chen, L. Guo, Z. Hea, L. Xia, G. Wang, P. Zhang. Y. No. J. Cryst. Growth, **515**, 66 (2019). DOI: 10.1016/j.jcrysgro.2019.03.016
[13] G. Song, D. Ma, X. Zhou, L. Wang, Z. Wei, C. Xu, S. Wang. High Pressure Res., **41**, 132 (2021).
[14] S. Eaton-Magaña, J.E. Shigley, C.M. Breeding. Gems & Gemology, **53** (3), 262 (2017). DOI: 10.5741/GEMS.53.3.262
[15] J.E. Shigley, S.F. McClure, C.M. Breeding, A. Hsi-tien Shen, S.M. Muhlmeister. G&G, **40** (2), 128 (2004). DOI: dx.doi.org/10.5741/GEMS.40.2.128
[16] E.Yu.Tonkov. *Fazovye diagrammy elementov pri vysokom davlenii* (Nauka, M., 1979) (in Russian)
[17] V.R. Regel, A.I. Slutsker, E.E. Tomashevsky. UFN, **106** (2), 193 (1972) (in Russian). DOI: 10.3367/UFNr.0106.197202a.0193
[18] A.I. Slutsker. FTT, **46** (9), 1606 (2004). (in Russian)
[19] L.B. Potapova *Mekhanika materialov pri slozhnom napryazhennom sostoyanii. Kak prognoziruyut predelnye napryazheniya-1,* M., 2005) (in Russian)
[20] V.V. Prut. ZhTF, **78** (5), 138 (2008). (in Russian)
[21] Kh. Khan. *Teoriya uprugosti: Osnovy lineinoi teorii i eyo primeneniya*, per c nem. (Mir, M., 1988) (in Russian).

Translated by E.Ilinskaya